Fuel 213 (2018) pp 215-221

EXPERIMENTAL INVESTIGATION OF THE EFFECT OF ORIFICES INCLINATION ANGLE IN MULTIHOLE DIESEL INJECTOR NOZZLES. PART 2 – SPRAY CHARACTERISTICS

Payri, R., Salvador, F.J. (*), De la Morena, J., Pagano, V.

CMT-Motores Térmicos. Universitat Politècnica de València, Spain

(*) Corresponding author:

Dr. F. Javier Salvador, fsalvado@mot.upv.es

CMT-Motores Térmicos, Universitat Politècnica de València

Camino de Vera s/n, E-46022 Spain.

Telephone: +34-963879658

FAX: +34-963877659

ABSTRACT

Diesel spray development is a key research topic due to its impact on the combustion characteristics. On the current paper, the effect of the orifices inclination angle on the spray penetration characteristics is evaluated. For this purpose, three nozzles with included angles of 90, 140 and 155 degrees are selected. Visualization tests are performed on a room-temperature constant-pressure vessel pressurized with a high-density gas (SF_6), in order to reproduce the density conditions inside the combustion chamber at the start of the injection event. Both frontal and lateral Mie-scattering visualization are used, depending on the particular nozzle configuration. Results show how the spray penetration is slower as the inclination angle increases, which is linked to its lower nozzle outlet

velocity. A statistical correlation of the spray penetration as a function of the area and velocity coefficients is obtained and discussed.

KEYWORDS: nozzle, Diesel, inclination, spray, visualization

NOMENCLATURE

a-d	Coefficients for the spray penetration correlation
A_{eff}	Effective area
A_o	Geometrical area
C_a	Area coefficient
C_d	Discharge coefficient
C_v	Velocity coefficient
D_o	Geometrical nozzle diameter
k	Constant term for spray penetration correlations
K_u	Spray velocity constant
$\dot{m}$	Mass flow
$\dot{M}$	Momentum flux
P_b	Discharge pressure
P_i	Injection pressure
S	Spray penetration
S'	Spray penetration from image contour
t	Time after start of injection
u_{eff}	Outlet orifice effective velocity

u_{th}	Theoretical outlet orifice velocity, $u_{th} = \sqrt{\frac{2 \cdot (P_i - P_b)}{\rho_f}}$

Greek Symbols

α	Nozzle included angle
ΔP	Pressure drop, $\Delta P = P_i - P_b$
ρ_a	Ambient density
ρ_f	Fuel density
υ_f	Fuel kinematic viscosity
θ_u	Spray angle defined from the velocity profile

1. INTRODUCTION.

Many researchers have focused on the study of diesel spray characteristics over the last decades. Naber and Siebers [1] established that the inert spray penetration has two different stages: an initial one, where the spray penetration grows linearly with the time; and a second one characterized by a square-root temporal evolution. Payri et al. [2] showed a similar behavior, and related the transitional time between both stages to the moment at which the injection rate stops being affected by the needle position. On the contrary, Zhang and Hung [3] analyzed the transitional time as a combined function of inertial, viscous and surface tension forces. More recently, Kostas et al. [4] and Li and Xu [5] proposed that the experimental trend of the spray penetration before this transitional time was actually proportional to $t^{3/2}$ once the very first millimeters of the spray were properly captured.

Additionally, spray penetration is significantly dependent on the nozzle orifice geometry. Payri et al. [6] reported a higher spray penetration for a tapered orifice compared to a cylindrical one, linked to its higher effective outlet velocity. Boggavarapu and Ravikrishna [7] showed that enlarging the orifice inlet rounding radii was also effective to increase the tip penetration velocity. Both these effects are related to the increase of the spray momentum, which has been seen as the most important parameter to characterize the spray penetration [8]. The needle seat geometry has also shown a a significant impact on the spray [9]. Another important aspect is the ambient density, which tends to reduce spray tip velocity due to the combined effect of higher aerodynamic forces and a wider spray angle [10,11]. Eventually, the combination of high ambient density with ultra-high injection pressure may lead to the detection of shock wave phenomena in the spray tip area, affecting also the spray behavior [12,13]. Spray penetration is also affected by the fuel physical properties, mainly density, viscosity and surface tension [14–16].

Apart from the characteristics of spray penetration, it is important to take into account also the structure of the spray itself [18,19]. During its first stages, especially in high density conditions, the spray develops a mushroom-like structure due to the interaction of the liquid fuel with the ambient gas [19,20]. As the spray develops, its structure transitions to a nearly conical shape, where the spray angle can be defined, followed by a semi-spherical tip. A high resolution analysis of the first millimeters of the spray shows that in reality there is a transitional region until reaching the spray angle [21–23]. X-ray visualization techniques have allowed to obtained the mass fraction radial distribution inside the spray [24–26], characterized by similar Gaussian profiles to those typical of gas jets [24,27]. When the spray is injected into evaporative (high temperature)

conditions, it has to be considered also that full spray evaporation is reached after a certain distance from the nozzle tip. This distance is called stabilized liquid length, and depends mostly on the orifice effective outlet diameter, the spray angle, the fuel properties and the ambient temperature [28–32].

Significant effort has been also made in the modeling of diesel sprays [33–36]. One-dimensional phenomenological models, based on the gaseous jet analogy, have shown to be useful to evaluate the main spray features both in stationary and transient conditions [37,38]. Nevertheless, microscopic details of the spray such as the droplet velocity and diameter or the turbulence characteristics cannot be evaluated using these methodologies. For this reason, full Computational Fluid-Dynamic (CFD) tools have been developed. Most of the available models have been based on Reynold-Averaged Navier-Stokes equations (RANS), which use simplified turbulence models able to capture only the average spray behavior [39–42]. In the last years, more advanced methodologies based on Large Eddy Simulation (LES) or Direct Numerical Simulation (DNS), capable to capture also spray cyclic oscillations, have also been investigated [43–45].

In the current paper, an investigation of the effect of nozzle inclination angle on the spray characteristics is performed. For this purpose, three multi-hole nozzles with different included angle are assessed. The nozzles were previously evaluated from the point of view of their hydraulic performance in terms of mass flow and momentum flux [46]. Spray penetration is obtained based on lateral and frontal Mie-scattering visualization. Results show that spray penetration is slightly faster as the included angle decreases. Additionally, a correlation of the spray penetration based on the area and velocity coefficients is obtained.

As far as the structure of the paper is concerned, the work is divided in 5 sections. Section 2 describes the experimental arrangement, including an uncertainty analysis as a function of the included angle for the frontal visualization. The main spray penetration results are depicted in Section 3. A theoretical analysis of the spray penetration is performed in Section 4, leading to the generation of a statistical correlation for the experimental data available. Finally, the main conclusions of the study are drawn in Section 5.

2. EXPERIMENTAL SETUP.

2.1. Nozzles

In the current paper, three fuel nozzles with included angle values of the included angle α = 90 (N1), α = 140 (N2) and α = 155 degrees (N3) have been used. These nozzles are equal from the point of view of the number of holes (10), nominal outlet diameter (D_o=0.09 mm), conicity (*k-factor*=1.5) and hydrogrinding level (10%), and are mounted on a solenoid-driven fuel injector. This injector is connected to a custom-made common-rail system capable to reach up to 200 MPa of injection pressure

2.2. Spray visualization

Spray visualization tests have been performed at room temperature on a constant-pressure test rig capable to reach up to 0.8 MPa. In order to work with ambient densities similar to those characteristic of the combustion chamber in a diesel engine, the test rig is filled with a gas denser than air. In particular, sulphur hexafluoride (SF_6) has been used. This gas is provided to the test rig by a roots compressor with a nominal flow velocity of 3 m/s, enough to facilitate the dragging of the fuel droplets from one injection cycle to another without impairing spray penetration.

As stated before, SF_6 was selected as the working gas in order to match the desired chamber density at pressure levels acceptable for the test rig (which are lower than the standard engine conditions). It has to be highlighted that this could have an effect on the nozzle flow characteristics due to the different pressure drop across the nozzle. This effect could be particularly important if cavitation took place in the orifices. Nevertheless, considering that no cavitation was observed during the previous hydraulic characterization of the nozzles [46], the expected impact is minor.

Mie-scattering technique is used to visualize the liquid spray penetration. For this particular arrangement illumination is provided by a high-intensity Xenon flashlight. The light scattered by the droplets is registered with a high-resolution CCD camera (PCO SensiCam). Both the flashlight and the camera are synchronized with the fuel injection event, capturing images every 20 µs. Five repetitions for the whole injection event have been registered.

Traditionally, Mie-scattering is setup in a frontal view configuration for diesel multi-hole injectors [47–49]. In this configuration, the sensor of the camera is placed in a perpendicular plane with respect to the fuel injector axis, allowing the simultaneous visualization of multiple sprays in a single image. A schematic of this configuration can be seen in Figure 1.a.

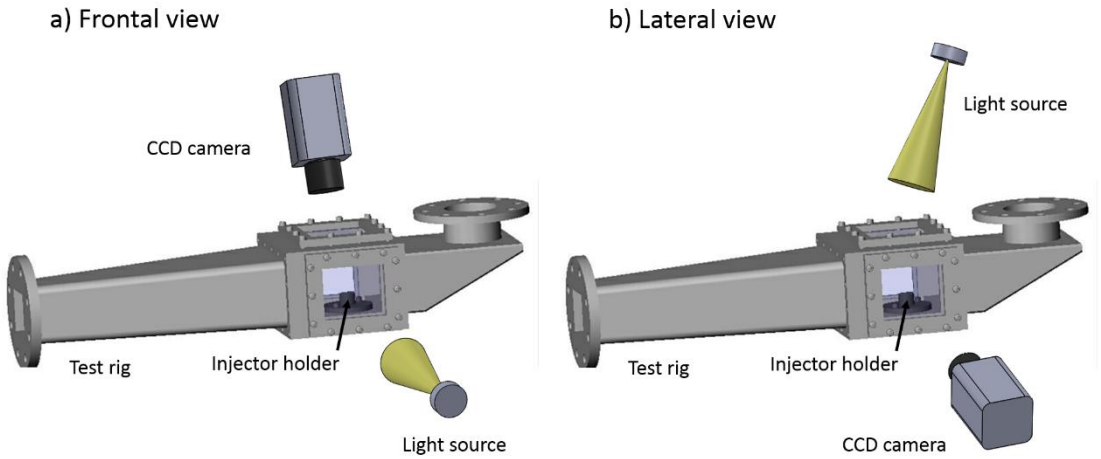

Fig. 1 Schematic of visualization configurations: a) frontal view; b) lateral view.

When using a frontal view in multi-hole injectors, it is necessary to take into account that there is an angle between the spray and the camera, which depends on the included angle. This can be better understood looking at Figure 2.

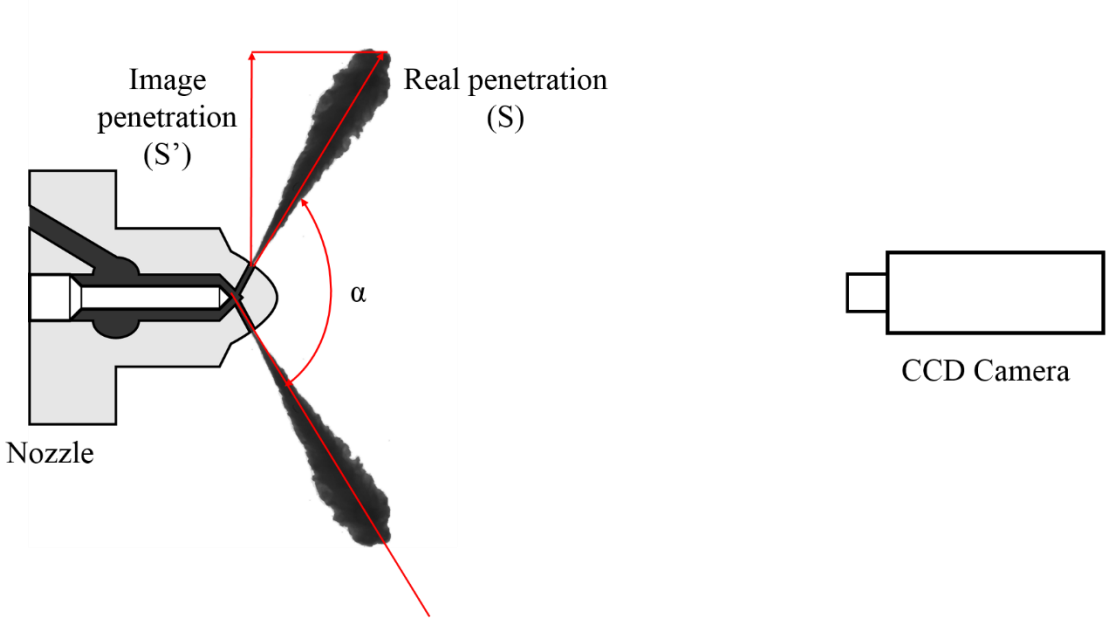

Fig. 2 Diagram for spray penetration determination in frontal view configuration.

In this figure, a diagram representing the frontal view configuration is seen. In this arrangement, the penetration obtained from the spray contour (*S'*) is a projection of the

real spray penetration (S) on a plane parallel to the CCD camera sensor. Consequently, the penetration can be calculated as:

$$S = \frac{S'}{\cos\left(90 - \frac{\alpha}{2}\right)} \quad (1)$$

This correction poses an extra uncertainty in the determination of the spray penetration. Indeed, any uncertainty in the determination of the spray contour is amplified in terms of the spray penetration quantification by a factor of $1/\cos\left(90 - \frac{\alpha}{2}\right)$. Consequently, higher included angles mean a stronger effect of this correction. This phenomenon can be seen in higher details in Figure 3, where the increase of the uncertainty is plotted against the included angle (starting from the ideal case of included angle 180º, where no correction would be applied).

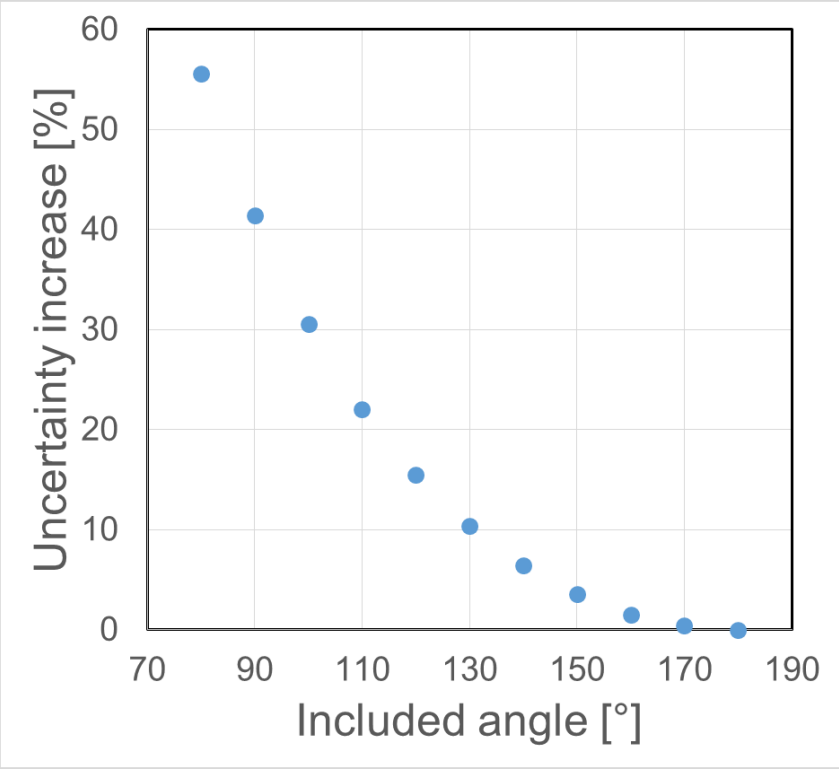

Fig. 3 Uncertainty increase in the spray penetration for the frontal view as a function of the nozzle included angle.

For the particular case of nozzle N1 in this study (α=90º) the increase in the uncertainty when using the frontal view would be higher than 40%, while the value is significantly lower for the other two nozzles (6.5 and 2% for nozzles N2 and N3, respectively). For the purpose of the current study, the effect of this higher correction was not considered acceptable. For this reason, this nozzle has been evaluated using a lateral view, as the one highlighted in Figure 1.b, where the injector has been rotated to ensure that one of the spray plumes was located in a plane parallel to the camera (i.e. no correction would be applied). Figure 4 shows an example of the kind of images obtained in both configurations.

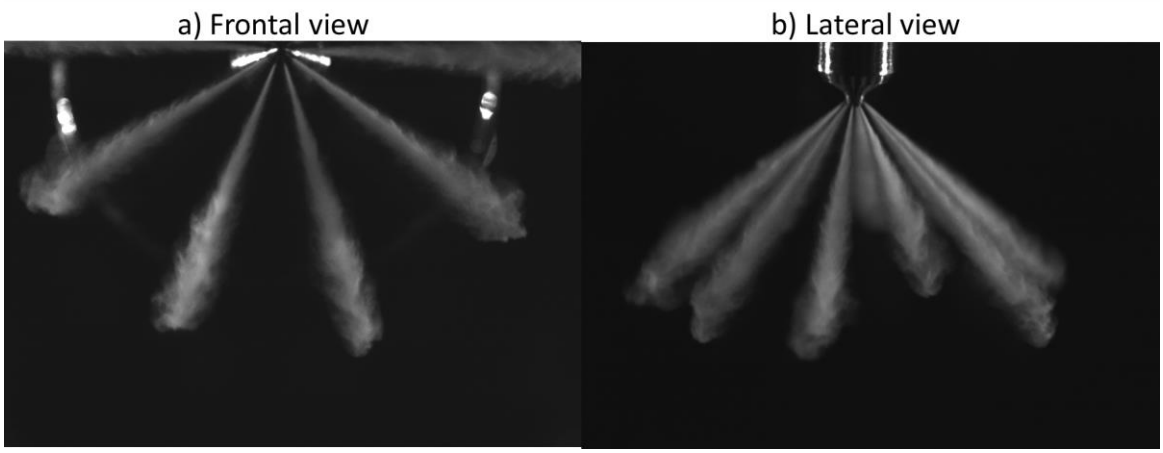

Fig. 4 Sample Mie-scattering images: a) frontal view; b) lateral view.

Unfortunately, as it can be seen from the image, the usage of lateral view configuration coupled with a large number of holes implies certain level of overlap between the spray plumes in the image, making harder the determination of the spray cone angle.

Once the images are obtained for either configuration, they have to be post-processed to determine the spray contour and the corresponding spray penetration. For this purpose, a background image is first subtracted, in order to eliminate reflections from the nozzle tip or other elements in the vessel. Then, a statistical analysis based on log-likelihood ratio

[50] of the resulting image determines a threshold for each image which distinguishes between spray and background information. From this threshold, the spray contour is obtained. Finally, the spray penetration is determined as the maximum distance between the spray tip and the nozzle orifice location.

The test matrix for the visualization study includes 8 levels of injection pressure from 23 to 200 MPa (the same ones already seen for the hydraulic tests presented in [46]) at an ambient density of 50 kg/m^3. The energizing time for these tests has been fixed at 1.5 ms for all the cases.

3. SPRAY PENETRATION RESULTS

An example of the result from the post-processing of the five repetitions taken in terms of spray penetration is seen in Figure 5 for nozzle N2 a point of 80 MPa. As it can be seen, good repeatability is observed between the different injection events, with a maximum deviation of approximately ±0.5mm. Similar results are obtained for other injectors and conditions. As a consequence, average values of the five repetitions will be considered from this point.

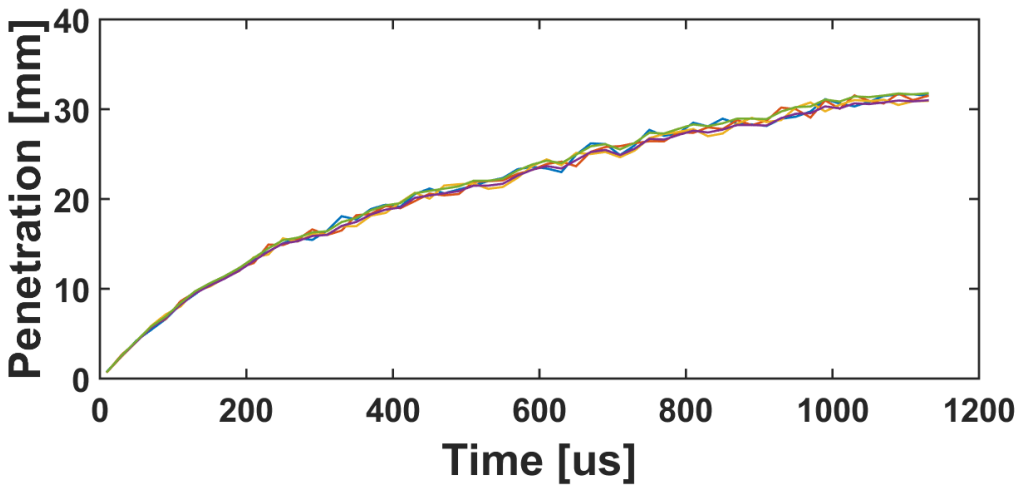

Fig. 5. Sample spray penetration results obtained for each repetition for N2 at 80 MPa.

Figure 6 shows the spray penetration results for the cases of 23 MPa (left) and 80 MPa (right). In order to facilitate the analysis, the spray penetration has been plotted together with the spray momentum data reported in [46].

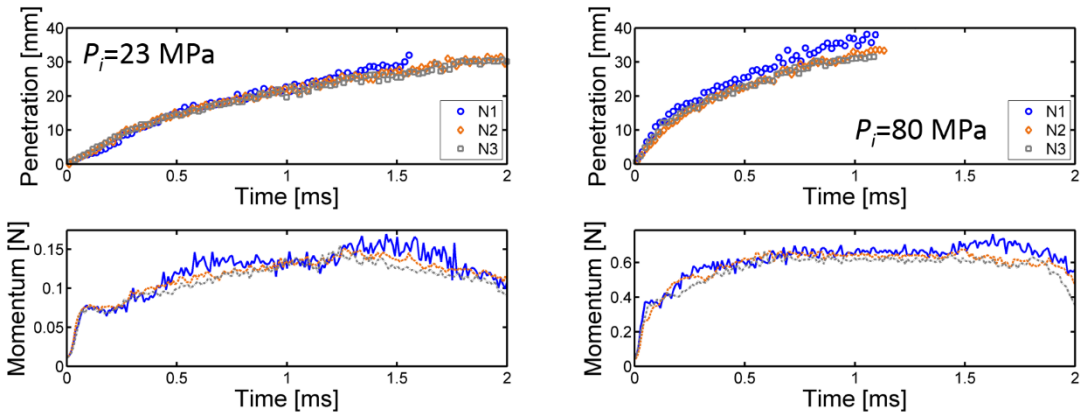

Fig. 6 Spray penetration results for injection pressures of 23 and 80 MPa.

As it can be seen, in both cases the spray penetration is faster for nozzle N1, which has the highest spray momentum. In the case of 23 MPa, penetration curves tend to diverge more after 1.2 ms from the start of injection, where a bump in the spray momentum was observed. For the 80 MPa condition, penetration is more consistently higher for N1. Regarding the other two nozzles, spray penetration is very similar for both of them, although the trend of reducing spray penetration when increasing the included angle is still appreciable. The relatively low differences between the nozzles is likely due to the effect of the inclination angle on the inlet rounding radii produced during the hydrogrinding process, as already discussed in [46]. The maximum spray penetration observed in the images is related to the arrival of the spray tip to the end of the visualization window. In nozzle N1, this value is higher due to the usage of the lateral view configuration. For the other two nozzles, both performed with frontal view, the optical limit is around 28 mm in terms of image penetration, resulting in slightly different maximum penetrations depending on the particular included angle value. Similar

conclusions can be established for the 120 and 200 MPa conditions, which are depicted in Figure 7.

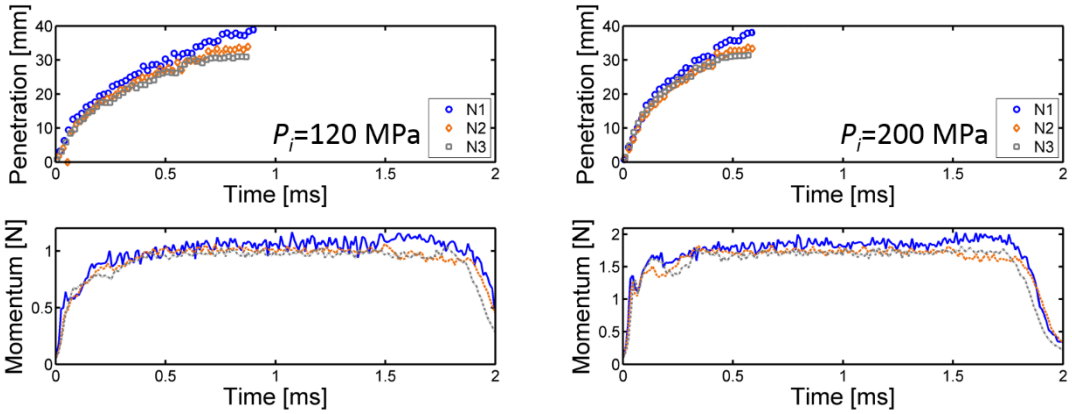

Fig. 7 Spray penetration results for injection pressures of 120 and 200 MPa.

4. STATISTICAL CORRELATIONS

As stated in the introduction, spray penetration shows a different behavior for the initial and fully-developed conditions. For the first stages of the injection event (up to approximately 10-12 millimeters), the spray penetration increases with time with an exponent going between 1 [1,51] and 1.5 [4,5], depending on the particular study considered. Additionally, the spray tip velocity is mostly a function of the pressure drop across the injector ($\Delta P = P_i - P_b$), which controls both the needle lift movement and the internal flow velocity, and the fuel-air density ratio. For this reason, the following correlation has been searched for this region of the spray:

$$S[mm] = k \cdot \Delta P^a[MPa] t^b[\mu s] \quad (2)$$

It has to be noted that the density ratio was not considered inside the correlation, since fuel and air density were maintained constant along the study. Table 1 shows a summary

of the results of the statistical analysis for the spray penetration in this near-nozzle region. Similar values were obtained by the authors in previous works [2].

Table 1. Summary of statistical correlations for the near-nozzle spray penetration.

Parameter	***Value***	***Interval of Confidence***
k	$9.9 \cdot 10^{-3}$	$[6.3 \cdot 10^{-3}, 1.35 \cdot 10^{-2}]$
a	0.593	[0.56,0.63]
b	0.95	[0.9,0.99]
R-squared	94.5%	

Figure 8 represents the observed vs. predicted spray penetration data corresponding to the correlation just obtained. As it can be seen, most of the data points are close to the ideal (diagonal) line, confirming the suitability of the correlation found to predict the experimental data. This can also be seen considering the relatively high R-squared value achieved (94.5%). Nevertheless, there is still some deviation appreciable, especially in the case of N1, which may be an indicator that there are secondary effects of the nozzle orifice inclination on the atomization and mixing processes that cannot be captured with the formulation proposed in equation (2).

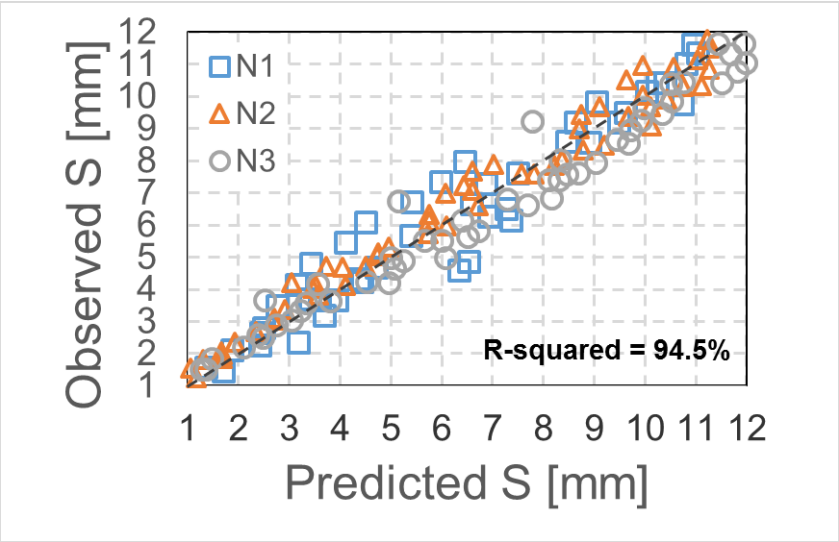

Fig. 8 Observed vs. predicted values for spray penetration correlation in the near-nozzle field.

For the fully-developed region (corresponding to the steady-state phase of the injection rate and momentum flux results), Desantes et al. [8] proposed a formulation for the spray penetration as a function of the spray momentum based on a theoretical analysis:

$$S = \left(\frac{2 \cdot 4.605}{\pi}\right)^{\frac{1}{4}} \cdot \frac{2}{K_u} \cdot \dot{M}_o^{\frac{1}{4}} \cdot \rho_a^{-\frac{1}{4}} \cdot t^{\frac{1}{2}} \cdot tan^{-\frac{1}{2}}\left(\frac{\theta_u}{2}\right) \quad (3)$$

Where θ_u is the spray angle based on the radial velocity profile, and K_u is a constant linking the spray tip velocity with the axial velocity inside the spray, which was found to be equal to approximately 2.076. If the spray momentum is expressed as a function of the effective orifice outlet velocity (u_{eff}) and area (A_{eff}), the following expression for the spray penetration is obtained:

$$S = \left(\frac{2 \cdot 4.605}{\pi}\right)^{\frac{1}{4}} \cdot \frac{2}{K_u} \cdot A_{eff}^{\frac{1}{4}} \cdot u_{eff}^{\frac{1}{2}} \left(\frac{\rho_f}{\rho_a}\right)^{\frac{1}{4}} \cdot t^{\frac{1}{2}} \cdot tan^{-\frac{1}{2}}\left(\frac{\theta_u}{2}\right) \quad (4)$$

Introducing the definition of the area (C_a) and velocity (C_v) coefficients:

$$S = \left(\frac{2 \cdot 4.605}{\pi}\right)^{\frac{1}{4}} \cdot \frac{2}{K_u} \cdot C_a^{\frac{1}{4}} \cdot A_o^{\frac{1}{4}} \cdot C_v^{\frac{1}{2}} \cdot u_{th}^{\frac{1}{2}} \left(\frac{\rho_f}{\rho_a}\right)^{\frac{1}{4}} \cdot t^{\frac{1}{2}} \cdot tan^{-\frac{1}{2}}\left(\frac{\theta_u}{2}\right) \quad (5)$$

Where A_o is the nozzle orifice geometrical outlet area and u_{th} the theoretical outlet velocity calculated from Bernoulli's equation. Based on this analysis, and considering that in the current study A_o, ρ_a and ρ_f are held constant, the following correlation is proposed:

$$S[mm] = k \cdot C_a^a \cdot C_v^b \cdot u_{th}^c[m/s] \cdot t^d[\mu s] \quad (6)$$

Table 2 summarizes the values obtained for each of the coefficients on the spray penetration correlation. As it can be seen, values of the exponents corresponding to the theoretical velocity and the time are very close to the ones predicted by equation (5). In the case of the exponents for the area and velocity coefficients, the values are still near the theoretical expectations, but some deviation appears. This deviation may be partially linked to the influence of these two parameters on the spray angle [52, 53]. In the current study, the spray angle could not be considered into the correlation due to the impossibility to have a proper spray angle characterization for the lateral visualization performed for nozzle N1.

Table 2. Summary of statistical correlations for the far field spray penetration

Parameter	***Value***	***Interval of Confidence***
k	$2.39 \cdot 10^{-2}$	$[2.1 \cdot 10^{-2}, 2.7 \cdot 10^{-2}]$
a	0.285	[0.23,0.34]
b	0.63	[0.62,0.64]
c	0.55	[0.51,0.59]
d	0.52	[0.51,0.53]
R-squared	95.8%	

Finally, Figure 9 shows the observed vs. experimental values for the far-field spray penetration. The high R-squared value (95.8 %) shows that there is a good agreement between the experimental measurements and the correlation proposed in this study.

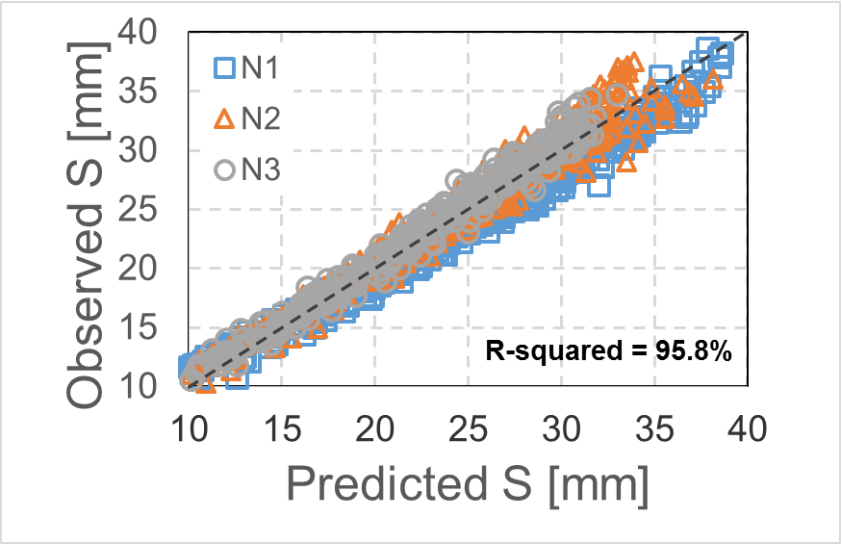

Fig. 9 Observed vs. predicted values for spray penetration correlation in the far-field.

It has to be highlighted that the accuracy of this correlation is significantly higher than the one previously analyzed for the near-nozzle field. This is related to the fact that the different nozzle flow characteristics related to the included angle could be captured. Unfortunately, this was not possible for the near-nozzle correlation for two main reasons. First, the uncertainties in the transient spray momentum determination made impossible to obtain the instantaneous values of C_a and C_v. Furthermore, the theoretical derivation leading to the last correlation, which is based on spray momentum conservation, is not applicable to the near-nozzle field since the spray momentum at the nozzle outlet is changing as the injector opens.

5. CONCLUSIONS

In the current paper, a study of the influence of the inclination angle of the nozzle orifices on the spray formation characteristics has been performed. For this purpose, three different nozzles with included angle values of 90, 140 and 155 degrees has been tested on a wide range of injection pressures (23-200 MPa). Spray penetration has been characterized using Mie-scattering visualization on a constant-pressure vessel at room temperature. For the 90 degrees nozzle, a lateral configuration has been used as opposed to the traditional frontal view used in diesel multihole injectors. This allowed to minimize the uncertainty in the spray penetration determination induced by the correction of the angle between the spray axes and the camera.

Results showed that lower included angle tends to produce faster spray penetration, since there are lower losses at the orifice entrance. This was consistent with the mass flow and momentum flux results previously obtained. Nevertheless, the differences were found to be limited thanks to the counter-acting effect of the rounding radii at the orifice inlet, which tend to be higher as the included angle increases. The effect of the included angle tended to be more visible as the injection pressure increases.

Statistical correlations have been searched for the spray penetration both in the initial and fully developed stages. During the first millimeters, spray penetration has been found to grow linearly with the time elapsed after the start of injection. Additionally, the pressure drop along the injector has shown to have a significant effect, with an exponent close to 0.6. Both results are consistent with previous works performed by the authors. Finally, in the fully developed field, spray penetration was correlated to the steady-state area and velocity coefficients, defined from mass flow and spray momentum. The final

297 coefficients were very close to the expectations from a theoretical analysis based on the
298 spray momentum.

299 **ACKNOWLEDGEMENTS.**

300 This work was partly sponsored by "*Ministerio de Economía y Competitividad*", of the
301 Spanish Government, in the frame of the Project "*Estudio de la interacción chorro-pared*
302 *en condiciones realistas de motor*", Reference *TRA2015-67679-c2-1-R.*

303 **References**

304 [1] Naber JD, Siebers DL. Effects of Gas Density and Vaporization on Penetration
305 and Dispersion of Diesel Sprays. SAE Pap. 960034, vol. 105, Society of
306 Automotive Engineers, Inc., Warrendale, Pennsylvania, USA; 1996, p. 82--111.
307 doi:10.4271/960034.

308 [2] Payri R, Salvador FJ, Gimeno J, Soare V. Determination of diesel sprays
309 characteristics in real engine in-cylinder air density and pressure conditions. J
310 Mech Sci Technol 2005;19:2040–52. doi:10.1007/BF02916497.

311 [3] Zhang G, Hung DLS. Temporal investigations of transient fuel spray
312 characteristics from a multi-hole injector using dimensionless analysis. Exp
313 Therm Fluid Sci 2015;66:150–9. doi:10.1016/j.expthermflusci.2015.03.011.

314 [4] Kostas J, Honnery D, Soria J. Time resolved measurements of the initial stages of
315 fuel spray penetration. Fuel 2009;88:2225–37. doi:10.1016/j.fuel.2009.05.013.

316 [5] Li Y, Xu H. Experimental study of temporal evolution of initial stage diesel spray
317 under varied conditions. Fuel 2016;171:44–53. doi:10.1016/j.fuel.2015.12.023.

318 [6] Payri R, Viera JP, Gopalakrishnan V, Szymkowicz PG. The effect of nozzle
319 geometry over internal flow and spray formation for three different fuels. Fuel
320 2016;183:20–33. doi:10.1016/j.fuel.2016.06.041.

321 [7] Boggavarapu P, Ravikrishna R V. A comparison of diesel and jatropha methyl
322 ester (JME) spray characteristics: effect of nozzle entry radius. At Sprays
323 2016;26:961–82.

324 [8] Desantes JM, Payri R, Salvador FJ, Gil A. Development and validation of a
325 theoretical model for diesel spray penetration. Fuel 2006;85:910–7.

326 [9] Bermúdez V, Payri R, Salvador FJ, Plazas AH. Study of the influence of nozzle
327 seat type on injection rate and spray behavior. ImechE J Automob Eng
328 2005;219:677–89. doi:10.1243/095440705X28303.

329 [10] Reitz RD, Bracco F V. On the dependence of spray angle and other spray
330 parameters on nozzle design and operating conditions. SAE Pap 790494 1979.
331 doi:10.4271/790494.

332 [11] Delacourt E, Desmet B, Besson B. Characterisation of very high pressure Diesel
333 sprays using digital imaging techniques. Fuel 2005;84:859–67.
334 doi:10.1016/j.fuel.2004.12.003.

335 [12] Jia TM, Li GX, Yu YS, Xu YJ. Effects of ultra-high injection pressure on
336 penetration characteristics of diesel spray and a two-mode leading edge shock
337 wave. Exp Therm Fluid Sci 2016;79:126–33.
338 doi:10.1016/j.expthermflusci.2016.07.006.

339 [13] Huang W, Wu Z, Gao Y, Zhang L. Effect of shock waves on the evolution of

high-pressure fuel jets. Appl Energy 2015;159:442–8. doi:10.1016/j.apenergy.2015.08.053.

[14] Kim D, Martz J, Violi A. Effects of fuel physical properties on direct injection spray and ignition behavior. Fuel 2016;180:481–96. doi:10.1016/j.fuel.2016.03.085.

[15] Som S, Longman DE, Ramirez AI, Aggarwal SK. Influence of Nozzle Orifice Geometry and Fuel Properties on Flow and Cavitation Characteristics of a Diesel Injector. Fuel Inject. Automot. Eng., InTech; 2012, p. 112–26. doi:10.5772/38900.

[16] Agarwal AK, Chaudhury VH. Spray characteristics of biodiesel/blends in a high pressure constant volume spray chamber. Exp Therm Fluid Sci 2012;42:212–8. doi:10.1016/j.expthermflusci.2012.05.006.

[17] Linne M. Imaging in the optically dense regions of a spray: A review of developing techniques. Prog Energy Combust Sci 2013;39:403–40. doi:10.1016/j.pecs.2013.06.001.

[18] Salvador FJ, Romero J V., Roselló MD, Jaramillo D. Numerical simulation of primary atomization in diesel spray at low injection pressure. J Comput Appl Math 2016;291:94–102.

[19] Crua C, Heikal MR, Gold MR. Microscopic imaging of the initial stage of diesel spray formation. Fuel 2015;157:140–50. doi:10.1016/j.fuel.2015.04.041.

[20] Ding H, Wang Z, Li Y, Xu H, Zuo C. Initial dynamic development of fuel spray analyzed by ultra high speed imaging. Fuel 2016;169:99–110.

362 doi:10.1016/j.fuel.2015.11.083.

363 [21] Desantes JM, Payri R, Salvador FJ, De la Morena J. Influence of cavitation
364 phenomenon on primary break-up and spray behavior at stationary conditions.
365 Fuel 2010;89:3033–41. doi:10.1016/j.fuel.2010.06.004.

366 [22] Payri R, Salvador FJ, Gimeno J, De la Morena J. Analysis of Diesel spray
367 atomization by means of a near-nozzle field visualization technique. At Sprays
368 2011;21:753–74. doi:10.1615/AtomizSpr.2012004051.

369 [23] Wang Z, Li Y, Wang C, Xu H, Wyszynski ML. Experimental study on primary
370 breakup of diesel spray under cold start conditions. Fuel 2016;183:617–26.
371 doi:10.1016/j.fuel.2016.06.067.

372 [24] Ramírez AI, Som S, Aggarwal SK, Kastengren AL, El-Hannouny EM, Longman
373 DE, et al. Quantitative X-ray measurements of high-pressure fuel sprays from a
374 production heavy duty diesel injector. Exp Fluids 2009;47:119–34.
375 doi:10.1007/s00348-009-0643-4.

376 [25] Moon S, Komada K, Sato K, Yokohata H, Wada Y, Yasuda N. Ultrafast X-ray
377 study of multi-hole GDI injector sprays: Effects of nozzle hole length and
378 number on initial spray formation. Exp Therm Fluid Sci 2015;68:68–81.
379 doi:10.1016/j.expthermflusci.2015.03.027.

380 [26] Desantes JM, Salvador FJ, Lopez JJ, De la Morena J. Study of mass and
381 momentum transfer in diesel sprays based on X-ray mass distribution
382 measurements and on a theoretical derivation. Exp Fluids 2011;50:233–46.
383 doi:10.1007/s00348-010-0919-8.

384 [27] Salvador FJ, Ruiz S, Gimeno J, De la Morena J. Estimation of a suitable Schmidt
385 number range in diesel sprays at high injection pressure. Int J Therm Sci
386 2011;50:1790–8. doi:10.1016/j.ijthermalsci.2011.03.030.

387 [28] Siebers DL. Scaling liquid-phase fuel penetration in diesel sprays based on
388 mixing-limited vaporization. SAE Tech Pap 1999-01-0528 1999.
389 doi:10.4271/1999-01-0528.

390 [29] Payri R, Gimeno J, De la Morena J, Battiston PA, Wadhwa A, Straub R. Study of
391 new prototype pintle injectors for diesel engine. Energy Convers Manag
392 2016;122:419–27. doi:10.1016/j.enconman.2016.06.003.

393 [30] Payri R, Salvador FJ, Gimeno J, De la Morena J. Influence of injector technology
394 on injection and combustion development, Part 2: Combustion analysis. Appl
395 Energy 2011;88:1130–1139.

396 [31] Martínez-Martínez S, Sánchez-Cruz FA, Riesco-Ávila JM, Gallegos-Muñoz A,
397 Aceves SM. Liquid penetration length in direct diesel fuel injection. Appl Therm
398 Eng 2008;28:1756–62. doi:10.1016/j.applthermaleng.2007.11.006.

399 [32] Pickett LM, Genzale CL, Manin J. Uncertainty quantification for liquid
400 penetration of evaporating sprays at diesel-like conditions. At Sprays
401 2015;25:425–52. doi:10.1615/AtomizSpr.2015010618.

402 [33] Reitz RD, Rutland CJ. Development and Testing of Diesel-Engine Cfd Models.
403 Prog Energy Combust Sci 1995;21:173–96. doi:Doi 10.1016/0360-
404 1285(95)00003-Z.

405 [34] Som S, Aggarwal SK. Effects of primary breakup modeling on spray and

406 combustion characteristics of compression ignition engines. Combust Flame
407 2010;157:1179–93. doi:10.1016/j.combustflame.2010.02.018.

408 [35] Ning W, Reitz RD, Diwakar R, Lippert AM. An eulerian-lagrangian spray and
409 atomization model with improved turbulence modeling. At Sprays 2009;19:727–
410 39.

411 [36] Salvador FJ, Gimeno J, Pastor JM, Martí-Aldaraví P. Effect of turbulence model
412 and inlet boundary condition on the diesel spray behavior simulated by an
413 eulerian spray atomization (ESA) model. Int J Multiph Flow 2014;65:108–16.
414 doi:10.1016/j.ijmultiphaseflow.2014.06.003.

415 [37] Salvador FJ, Ruiz S, Salavert JM, De la Morena J. Consequences of using
416 biodiesel on the injection and air-fuel mixing processes in diesel engines. Proc
417 Inst Mech Eng Part D J Automob Eng 2013;227:1130–41.
418 doi:10.1177/0954407012463667.

419 [38] Dhar A, Tauzia X, Maiboom A. Phenomenological models for prediction of
420 spray penetration and mixture properties for different injection profiles. Fuel
421 2016;171:136–42. doi:10.1016/j.fuel.2015.12.022.

422 [39] Lee CH, Reitz RD. CFD simulations of diesel spray tip penetration with multiple
423 injections and with engine compression ratios up to 100:1. Fuel 2013.
424 doi:10.1016/j.fuel.2013.04.058.

425 [40] Maghbouli A, Lucchini T, D'Errico G, Onorati A. Effects of grid alignment on
426 modeling the spray and mixing process in direct injection diesel engines under
427 non-reacting operating conditions. Appl Therm Eng 2015;91:901–12.

428 doi:10.1016/j.applthermaleng.2015.07.051.

429 [41] Kosters A, Karlsson A. Validation of the Vsb2 Spray Model Against Spray A and
430 Spray H. At Sprays 2016;26:775–98. doi:10.1615/AtomizSpr.2015011670.

431 [42] Tonini S, Gavaises M, Theodorakakos A. Modelling of high-pressure dense
432 diesel sprays with adaptive local grid refinement. Int J Heat Fluid Flow
433 2008;29:427–48. doi:10.1016/j.ijheatfluidflow.2007.11.009.

434 [43] Ghiji M, Goldsworthy L, Brandner PA, Garaniya V, Hield P. Analysis of diesel
435 spray dynamics using a compressible Eulerian/VOF/LES model and microscopic
436 shadowgraphy. Fuel 2017;188:352–66. doi:10.1016/j.fuel.2016.10.041.

437 [44] Zhou L, Luo KH, Qin W, Jia M, Shuai SJ. Large eddy simulation of spray and
438 combustion characteristics with realistic chemistry and high-order numerical
439 scheme under diesel engine-like conditions. Energy Convers Manag
440 2015;93:377–87. doi:10.1016/j.enconman.2015.01.033.

441 [45] Lebas R, Menard T, Beau PA, Berlemont A, Demoulin F-X. Numerical
442 simulation of primary break-up and atomization: DNS and modelling study
443 35:247–60. doi:10.1016/j.ijmultiphaseflow.2008.11.005.

444 [46] Salvador FJ, Lopez JJ, De la Morena J, Crialesi-Esposito M. Experimental
445 investigation of the effects of orifices inclination angle on multihole diesel
446 injector nozzles. Part 1 - hydraulic performance. Fuel 2017; In press;
447 doi:10.1016/j.fuel.2017.04.019.

448 [47] Adam A, Leick P, Bittlinger G, Schulz C. Visualization of the evaporation of a
449 Diesel spray using combined Mie and Rayleigh scattering techniques. Exp.

Fluids, vol. 47, Lisbon: 2009, p. 439–49. doi:10.1007/s00348-009-0673-y.

[48] Payri R, Salvador FJ, Garcia A, Gil A. Combination of visualization techniques for the analysis of evaporating diesel sprays. Energy & Fuels 2012;26:5481–90. doi:10.1021/ef3008823.

[49] Park Y, Hwang J, Bae C, Kim K, Lee J, Pyo S. Effects of diesel fuel temperature on fuel flow and spray characteristics. Fuel 2015;162:1–7. doi:10.1016/j.fuel.2015.09.008.

[50] Pastor JV, Arrègle J, Garcia-Oliver JM, Zapata LD. Segmentation of Diesel spray images with log-likelihood ratio test algorithm for non-Gaussian distributions. Appl Opt 2007;46:888–99. doi:10.1364/AO.46.000888.

[51] Payri R, Salvador FJ, Gimeno J, De la Morena J. Macroscopic behaviour of Diesel Sprays in the Near-Nozzle Field. SAE Tech Pap 2008-01-0929 2008.

[52] Payri R, Salvador FJ, Gimeno J, Novella R. Flow regime effects on non-cavitating injection nozzles over spray behavior. Int J Heat Fluid Flow 2010;32:273–284.

[53] Payri R, Salvador FJ, Gimeno J. Flow regime effects over non-cavitating diesel injection nozzles. Proceedings of the institution of mechanical engineers, Part-D-Journal of Automobile engineering, vol. 226, D1, pp. 133-144. 2012. doi: 10.1177/0954407011413056

471

472

473